https://doi.org/10.3311/PPci.41726

Periodica Polytechnica Civil Engineering

Development of the Numerical Model for Determining the Strength of High-profiled Sheets

Ivan Nešović[1*], Marina Mijalković[1], Todor Vacev[1], Miloš Milić[1], Marina Trajković Milenković[1], Andrija Zorić[1], Nikola Janković[1]

[1] Department of Civil Engineering, Faculty of Civil Engineering and Architecture, University of Niš, Aleksandra Medvedeva 14, 18000 Niš, Serbia
[*] Corresponding author, e-mail: ivan.nesovic@gaf.ni.ac.rs

Received: 26 July 2025, Accepted: 15 April 2026, Published online: 04 May 2026

Abstract

High-profiled sheets (HPS) are widely used in the construction of numerous building structures. The constant development of new forms of sheet profiling in order to optimize these elements compelled the designers to determine their strength, which is a complex process, especially if traditional analytical methods are used. On the other hand, the Finite Element Method (FEM) represents a good alternative to analytical calculations and experimental testing that require significant financial investments. However, the available information on the modeling of these structural elements is insufficient. This paper presents the development of a numerical model of HPS made of structural steel. The pronounced profile height causes a stability problem, so a geometrically and materially non-linear analysis with imperfections (GMNIA) was carried out. The developed numerical model should serve as a basis for further research into improving the manufacturer's data on strength of the HPS. The paper specifically addresses the influence of geometric imperfections on the strength. The shape and size of the imperfections were analyzed and their critical size leading to failure was determined. To confirm the reliability of the developed numerical model, load-bearing analyses were performed with varying the length of the contact area and the number of fasteners for connecting the HPS to the supporting structure. The developed numerical model showed very good agreement with the experimental analysis, carried out by author, both for the ultimate limit state and the serviceability limit state, so the numerical model was successfully validated.

Keywords

high-profiled sheet metal, strength, imperfection, nonlinear FEA, experimental research

1 Introduction

Use of the second generation high-profiled sheets metal (HPS) is widely present in civil engineering [1]. Owing to the quick and easy assembly they are especially used as structural elements for covering medium and large spans, independently or as a substructure for roof insulation. HPS can also work in conjunction with the main supporting structure of the building, enabling the so-called stressed skin concept [2, 3]. They are very often used as a permanent element of the formwork and as a substitution for the tensioned reinforcement in construction of the reinforced concrete floor slabs.

The cost-effectiveness of HPS girders is constantly improving, primarily through increasing the load-bearing capacity while retaining the same material consumption. This is most often achieved by optimizing the cross-sectional geometry. The methodology for determining and verifying the strength of HPS can vary, and is often based on analytical calculations regulated by national standards [4–6]. They are based on multi-parameter expressions that are often complicated for practical application. Experimental tests are regularly used and considered the most reliable method, however, their implementation requires significant resources in terms of finances and equipment. In addition to these two methods, it is also possible to apply a numerical analysis using the finite element method (FEM) and contemporary engineering software. This method provides the possibility of using nonlinear analysis in the geometric, material and contact domain, but also requires that the developed numerical model be experimentally validated. In addition, a special problem in developing a numerical model is the correct selection and input of geometric imperfections (GI), to which HPSs are particularly susceptible due to the small thickness of the base material

Cite this article as: Nešović, I., Mijalković, M., Vacev, T., Milić, M., Milenković, M. T., Zorić, A., Janković, N. "Development of the Numerical Model for Determining the Strength of High-Profiled Sheets", Periodica Polytechnica Civil Engineering, 2026. https://doi.org/10.3311/PPci.41726

and high slenderness, and which can occur during the production, manipulation or storage process [7]. Their presence increases the tendency for local loss of stability to occur even before the yield point is reached. Therefore, the analysis of the behavior and determination of the load-bearing capacity of cold-formed steel sections (CFS) due to the influence of GI has been the subject of numerous scientific studies [8–12]. A special problem is certainly the proper selection and inclusion of these influences when creating numerical models.

The numerical modeling procedure with the influence of GI on the analysis of nonlinear behavior of CFS was among the first demonstrated by Schafer et al. [13] and Schafer and Peköz [14]. He concluded that despite the known shortcomings, the presented modeling method has a significant potential for future research. Numerous researchers have subsequently used FEM to study the behavior of CFS under the influence of various loads [15–24]. The majority of them came to the conclusion that validation of the developed model can only be carried out after the introduction of GI. Casafont et al. [17] analyzed the behavior of a steel trapezoidal sheet (TS) by varying several parameters, including the GI input proposed by the standard CEN EN 1993-1-14:2025 [25]. Several combinations of GIs obtained based on the shape of the TS buckling were modeled and it was concluded that the obtained results only slightly differ from each other. In paper [21] the effects of three different GI sizes based on distortional and local elastic buckling of the top flange TS were analyzed. The authors concluded that the distribution and size of GI do not exhibit excessive differences in the load-bearing capacity of the developed numerical model of TS. In order to optimize the second generation of TS in the future, Szumigała [26] has validated the developed numerical model based on experimental testing of two types of HPS. The presented results show deviations of about 15% in terms of calculated load bearing capacity between these two methods, which may be a consequence of the neglected influence of the introduction of GI when developing the model. Other researchers have developed special methods (direct strength method) for determining the ultimate bearing capacity of the first and second generation of TSs [1, 27, 28]. Dogar [29] in his paper, performed an experimental-numerical analysis of determining the load-bearing capacity of type LTP 200 HPS in the Gerber support static system. Some manufacturers of TS [30] have developed simple software (Optimi) [31] for calculating the strength of their products, treating them as linear beams.

Most of the mentioned authors have analyzed in their papers the influence of a large number of parameters on the load-bearing capacity of TS (profile curvature radius, GI arrangement, GI size, method of load application, etc.) with less attention to the modeling methodology. For these reasons, the goal of this paper is to develop a reliable numerical model for determining the strength of HPS under bending. The modeling procedure was carried out in an advanced engineering software, Femap with NX Nastran [32], in accordance with the recommendations of the new standard CEN EN 1993-1-14:2025 [25]. Special attention is paid in the research to the influence of imperfections, which has been insufficiently investigated. Within this framework, a proposal for a methodology for introducing the equivalent geometric imperfection (EGI) is given. Individual results obtained with the participation of EGI are calibrated with appropriate experimental results. For a more detailed validation of the model, the paper analyzed the effects of the support contact length and the number of fasteners connecting HPS with the supporting structure. In that way the developed numerical model includes the effects of parameters that are not possible to consider using the analytical methods given in the standards. The overall analysis was performed on individual panels of the most commonly used type TR 153 HPS with a profile height of 153 mm and a covering width of 840 mm. The static system of the structure was assumed to be a beam with partially clamped ends, which is the most common case in engineering practice.

2 Experimental analysis

Seven HPS samples of TR 153 were tested, with a span of 6000 mm, with different supporting conditions, where the length of the contact area of the sheet and the support was varied, as well as the number and position of fasteners connecting the sheet metal to the support structure (Table 1). The supporting conditions that are most commonly used in practice have been selected.

Table 1 HPS samples and supporting conditions

Number	Sample label	Support area length B [mm]	Number of fasteners N [pcs.]
1	B40 N4	40	4
2	B80 N4	80	4
3	B120 N4	120	4
4	B160 N4	160	4
5	B200 N4	200	4
6	B160 N8	160	8
7	B200 N8	200	8

The fasteners used for connection of HPS and the purlin were M6×20…8.8 bolts, with a wide washer. The position of the bolts in the connection is illustrated in Fig. 1 (a) and (b). During the test, purlins were rested on auxiliary supports, anchored into a concrete slab.

The load was applied according to the recommendations of the Annex A of the standard CEN EN 1993-1-3:2006 [6], which stipulates a load application using four concentrated forces. This required the use of an additional structure (Fig. 2 (a) and (b)) to distribute the force from the press piston into four forces acting on the tested specimen. Due to small width of bottom flanges, the load is applied via the timber cross beams on the top flanges, which is also the most common case in practice. The proposed procedure is one of the most commonly used methods for testing sheets and panels [6, 17, 28, 29, 33–35].

The dead weight of the specimen, as well as the weight of the loading structure, was treated as an external load of 0.4 kN/m^2. The press load was applied in 1 kN increments, which is equivalent to a surface load of 0.2 kN/m^2. During the testing of the specimens, the deflection at

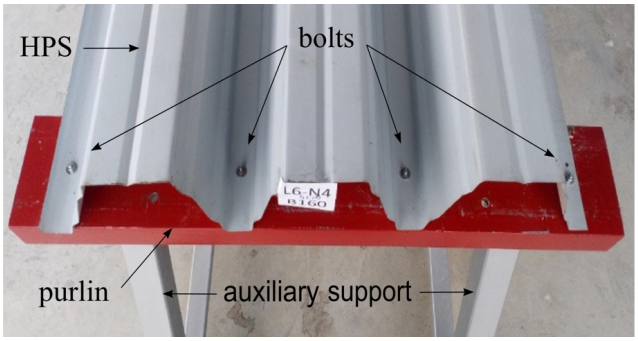

(a)

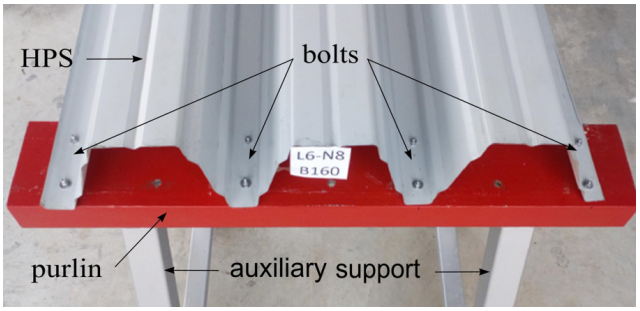

(b)

Fig. 1 Connection of the sheet and purlin: (a) with four bolts (sample B160 N4), (b) with eight bolts (sample B160 N8)

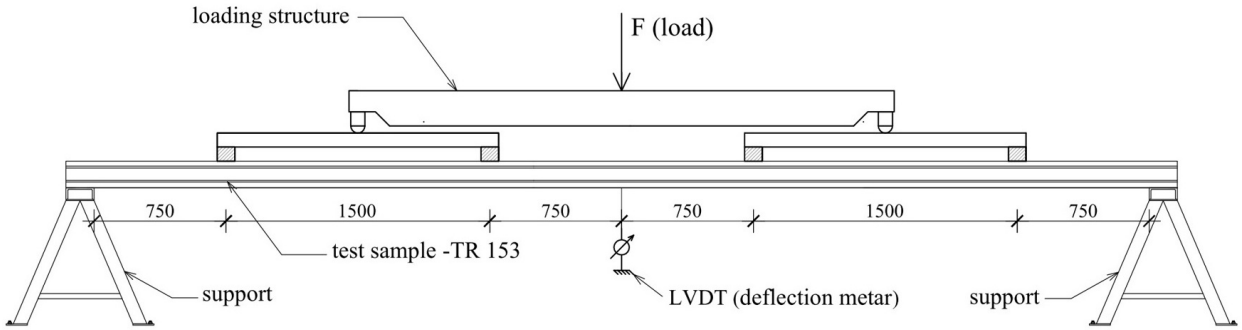

(a)

(b)

Fig. 2 Test setup: (a) disposition with the distribution of measuring points (measures in mm), (b) view of the specimen with the loading equipment

midspan was measured and the failure load was recorded. The location where the failure started and the propagation were clearly observable in all specimens. After reaching the ultimate load and observing the corresponding deflection, the load application is discontinued, because the additional abrupt increase of the deflection would damage the measuring equipment fitted under the specimen.

3 Development of the FEM model

The FE models fully correspond in shape and dimensions to the real specimens that have been experimentally tested. Although the samples have end lip only on one lower edge (Fig. 1), it was adopted that they have two planes of symmetry, because the size of the lip is rather small in respect to the dimensions of the cross-section. In addition, the lip is located in the tensioned part of the cross-section, so it has no significant effect on the mechanical characteristics and thereby on the analysis results. Because of that, only a quarter of the sample was modeled, with appropriate boundary conditions. This allows for simpler modeling and faster calculations. The modeling procedure is described in detail in the following text.

3.1 Selection of finite elements and material models

The numerical model consists of three components (Fig. 3). Table 2 lists the used components and types of finite elements (FE), as well as the corresponding material models.

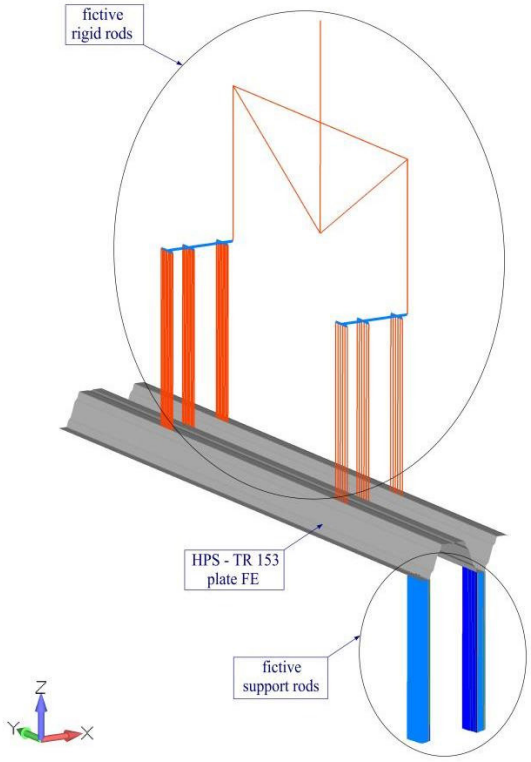

Fig. 3 Numerical models components

Table 2 Components of the numerical model, FE types and corresponding material models

No.	Modeling component/function	FE type	Material model
1	High-profiled sheet	4-node PLATE	Multilinear plastic
2	Fictive support rods	2-node ROD	Nonlinear elastic
3	Fictive rigid rods	2-node ROD	Linear elastic (rigid rods)

3.1.1 Profiled sheet modeling

Surface FE of the 4-node PLATE type, which have four corner nodes, were used. The modeling of the sheet metal bends was approximated by polygonal contours with flat plate elements placed along the curvature. Since plastic behavior of steel is expected in the vicinity of the supports, and in the points of load application, the mesh density increase was performed in these zones (Fig. 4 (c)).

Regarding the FE size, the FE model is divided in three zones:

- zones A with locally dense mesh in the vicinity of the supports and at the point of force application, where larger local deformations are expected, have a length of 90 mm;
- zones B with globally coarse mesh, where nonlinear behavior is not expected, are set in the rest of the structure;
- transition zones C form a gradual transition between the zone with dense mesh and the zone with coarse mesh.

The material model of the sheet metal was adopted based on laboratory testing of coupons obtained from the tested HPS panels (Table 3, Fig. 5). Measurements determined that the actual thickness of the sheet metal was 0.74 mm.

3.1.2 Modeling of supports

As a rule, two or more structural elements come into contact with each other at supports. Accordingly, a detailed analysis should also include this phenomenon. To implement the contact analysis, the modeling shown in Fig. 6 was performed. Namely, the contact between the bottom flange of HPS and the supporting structure (purlin) was implemented through fictive rods "support rods" denoted as type 1–4 (Fig. 6 (a)). These rods have negligible tensile stiffness and high compressive stiffness, which allows HPS to rest on the purlin, as well as to lift off due to rotation on the support. Fictive rods type 1 are placed at the bottom flanges which provide the contact with the purlin due to the self-weight of the HPS. Type 2–4 rods are placed in the nodes 2', 3' and 4' (Fig. 6 (b)) positioned on the fillet

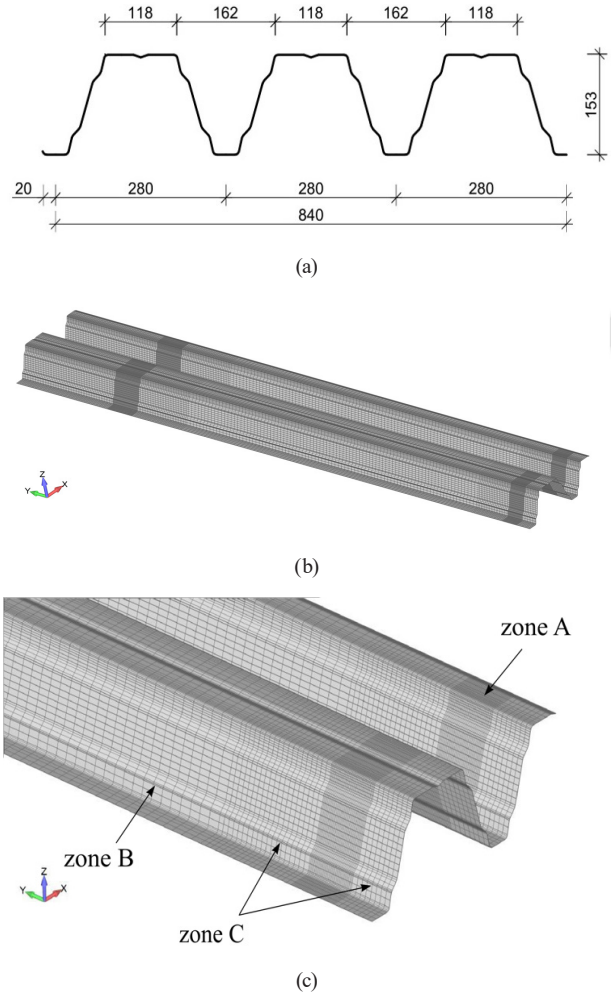

Fig. 4 HPS "TR 153": (a) cross section – geometry (measures in mm), (b) FE mesh – general appearance, (c) FE mesh – detail

Table 3 Steel material data

Part	Steel grade	Core thickness [mm]	Elasticity modulus [GPa]	Yield point [MPa]	Ultimate strength [MPa]
Steel sheet	S350	0.74	210	360	456

where the bottom flange transitions into the web. Their role as supports becomes active only after the annulling of the gaps Δ2, Δ3 and Δ4 due to the deformation.

Specific material models for rod types 1–4 were adopted according to the calculated strains after loading (Table 4). A characteristic diagram of the material model is shown in Fig. 7. The adopted modulus of elasticity is E = 2.1E+11 Pa, the cross-section area is $A = 10^{-4}$ m^2, and the length of the fictive rods is 1 m.

3.2 Boundary conditions, load and analysis course

Given the double symmetry of the FEM model, appropriate boundary conditions for loads and displacements have been introduced (Fig. 8).

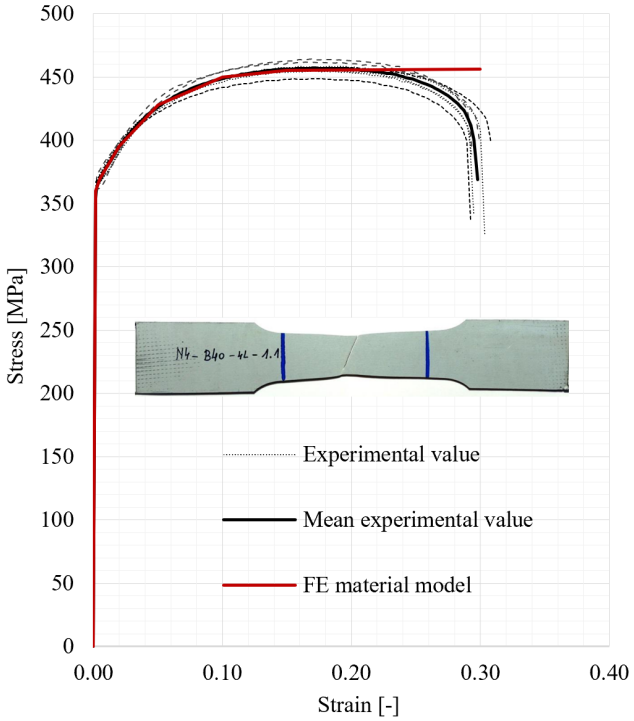

Fig. 5 Experimental stress-strain diagrams for steel material of the HPS

The load is applied in accordance with the conducted experimental research, i.e., by simulating the application of the load by a press device. For these reasons, an auxiliary structure has been modeled, according to the experimental setup in Fig. 2.

Model consists of a system of fictive rigid rods and the concentrated load applied from the press is distributed as the uniform line load acting at quarters of the model span (Fig. 8). The load is applied by displacing the node of the fictive rod 1. The adopted maximal displacement was 60 mm, because the conducted experimental testing has shown that this value is sufficient to achieve failure. The load is further transferred via the system of rods 3–5. The load is introduced into the sheet metal model in the nodes on the fillets between the web and the top flange. Such method of introduction of the load in the FE model is adopted based on the behavior of the specimen during the experimental analysis, where it was observed that the timber beams directly transfer the load only near bendings that are capable to accept the local compression (Fig. 9).

The connection of the sheet metal and the purlin is modeled with "bolt node" with restrained displacement in the X and Z directions (TX = TZ = 0). The displacement in the Y direction is free, because the results of the experiment indicated connection yield in this direction (hole ovalization) (Fig. 10).

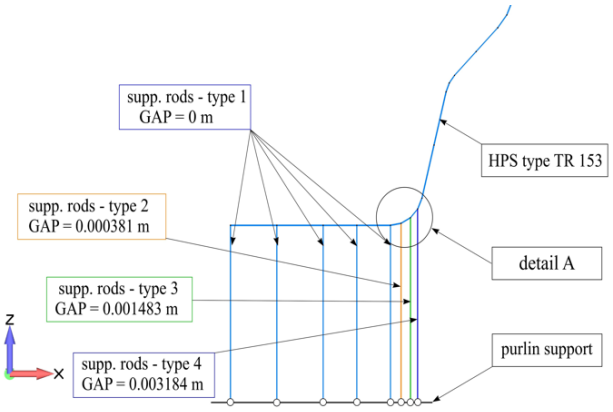

(a)

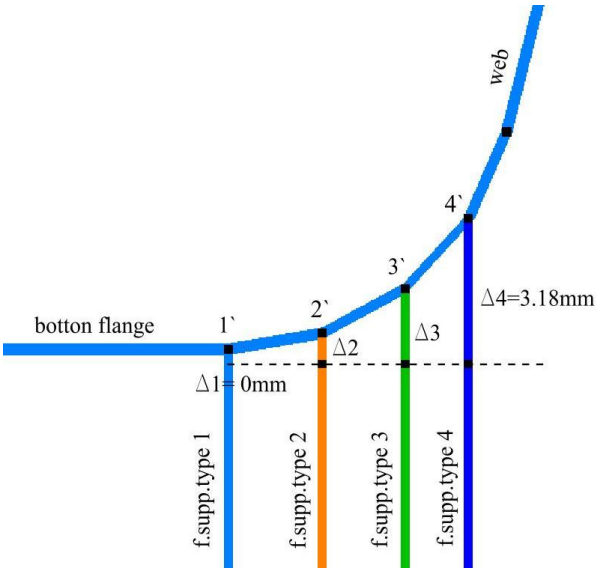

(b)

Fig. 6 (a) Fictive rods on the supporting zone of the bottom flange of HPS, (b) detail A

Table 4 Material data for support rods

Fictive rods				
	Type 1 gap Δ1 = 0 m		Type 2 gap Δ2 = 0.000381 m	
Point on diagram	Strain ε [−]	Stress σ [Pa]	Strain ε [−]	Stress σ [Pa]
A	−1.0	−2.1E11	−1.000381	−2.1E11
B	0.0	0.0	−0.000381	0.0
C	1.0	1.0	0.999619	1.0
	Type 3 gap Δ3 = 0.001483 m		Type 4 gap Δ4 = 0.003184 m	
Point on diagram	Strain ε [−]	Stress σ [Pa]	Strain ε [−]	Stress σ [Pa]
A	−1.001483	−2.1E11	−1.003184	−2.1E11
B	−0.001483	0.0	−0.003184	0.0
C	0.998517	1.0	0.996816	1.0

The displayed occurrence of bolt hole ovalization indicates the existence of a horizontal reaction.

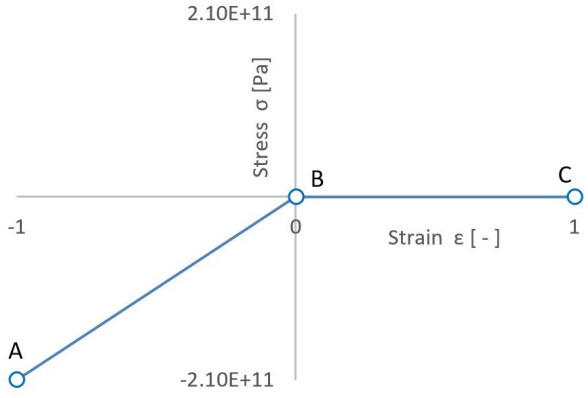

Fig. 7 Working diagram for the material of the fictive support rods (Type 1)

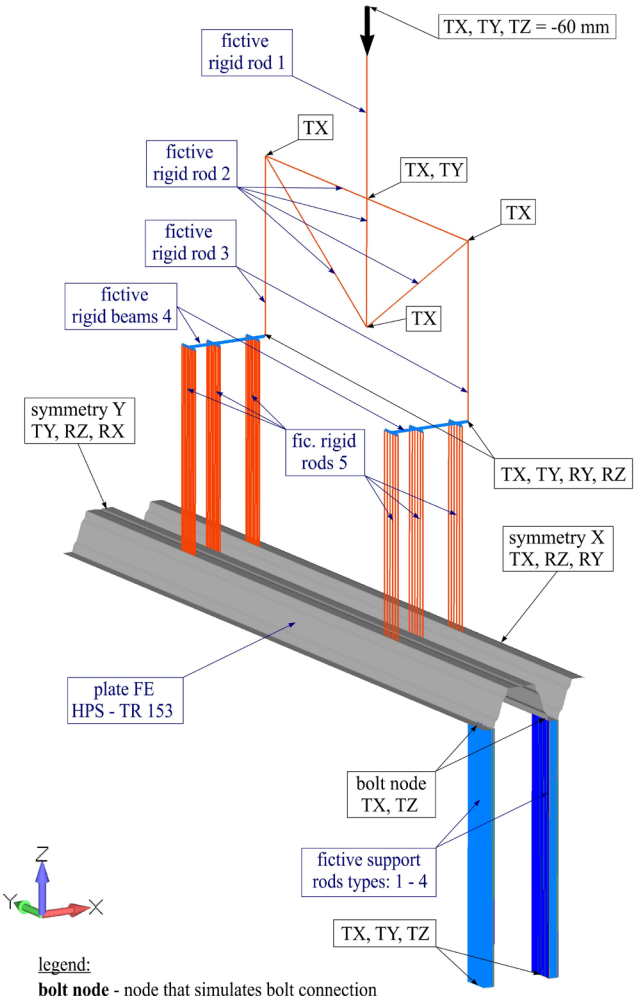

Fig. 8 Boundary conditions in the model: TX, TY, TZ restrained displacement in X, Y, Z directions respectively; RX, RY, RZ restrained rotations of about the X, Y, Z axes respectively

However, considering that the analyzed sheets are very thin (0.74mm), the resistance of these connections is low. For these reasons, the numerical model was simplified by not considering the impact of the bolt connections on the shear strength in the further analysis.

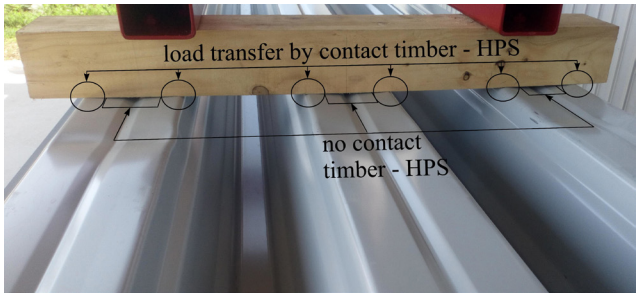

Fig. 9 Load transfer from timber beams on HPS

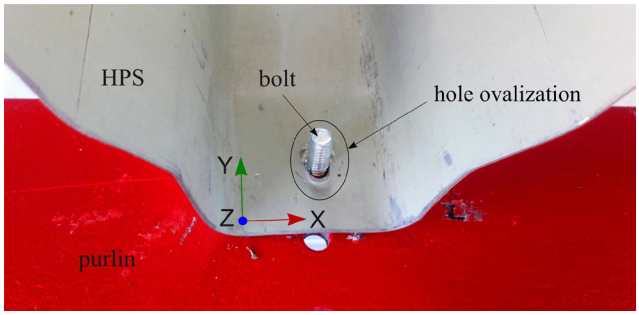

Fig. 10 Experimental analysis: bolt hole ovalization in the longitudinal (Y) direction at the support zone

For the FE model, a nonlinear static analysis with geometric and material nonlinearity was chosen. The load application was performed incrementally in 100 steps. This corresponds to a displacement of the press piston of 60/100 mm during the experimental test.

3.3 Verification and validation of the FEM models

Model verification was performed based on the results of the numerical FEM analysis, which included geometric and material nonlinearity (GMNA), and was performed for three different mesh densities. A model with a support contact length of 120 mm and four fasteners (B120 N4) was chosen as representative. Fig. 4 (b), (c), shows the model with the FEM medium mesh density, and Fig. 11 (a), (b), shows the models with coarse and fine mesh.

Data on the size of the FEs and their number are given in Table 5, together with the values of the calculated load bearing capacity and maximum deflections.

Based on the results presented in Table 5, good agreement is observed for all three mesh densities, so it can be considered that the developed model is verified. For further analysis, a medium size mesh was selected, which gives satisfactory results and does not require large computing resources.

The results of the numerical analysis were compared with the corresponding test results and are shown in Fig. 12. Fig. 12 demonstrates that the ultimate strength value obtained by applying FEM is about 23% higher than the value obtained by test analysis. Such large deviations

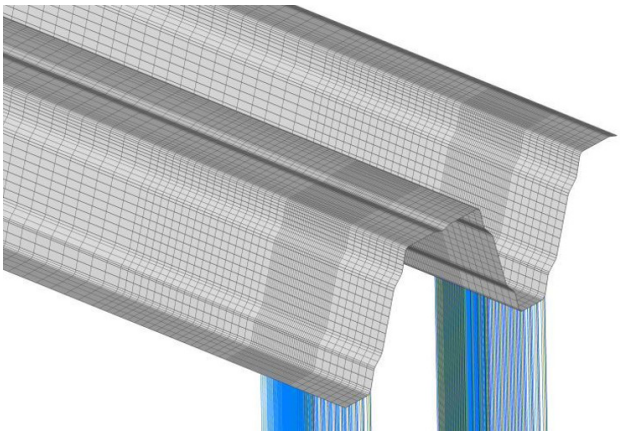

(a)

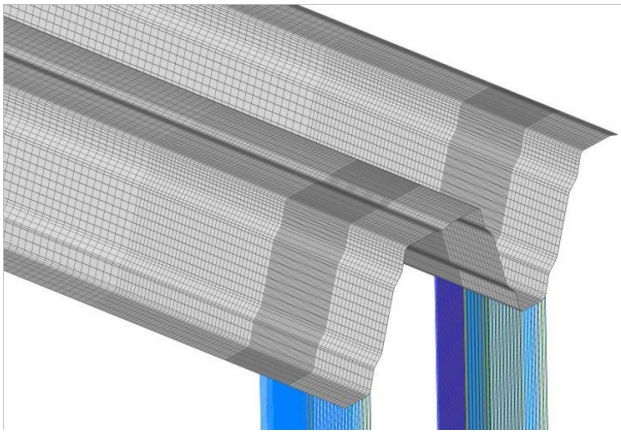

(b)

Fig. 11 FE mesh used for model verification (detail at support): (a) coarse, (b) fine

Table 5 Mesh sensitivity (bold values data adopted for further analysis)

	Mesh		
	Coarse	Medium	Fine
Number of nodes	23828	**44195**	77873
Number of FE	23574	**43804**	77256
Global FE size (mm)	40	**20**	10
Transition FE size (mm)	20	**10**	5
Local FE size (mm)	5	**2.5**	1.25
p_{ult} (kN/m^2)	3.23	**3.22**	3.22
w_{max} (mm)	86.77	**85.24**	84.90

indicate that additional improvement of the FEM model is necessary, in order to obtain a better agreement with the test and a successful validation of the developed FEM model. For that purpose, the behavior of the HPS at failure obtained by FEM and by test analysis was analyzed. It was observed that both methods give an identical failure mode (Fig. 13 (a)–(c)). Namely, the failure in both cases occurs in all three waves, in approximately the same cross section and at approximately the same distance from the load application

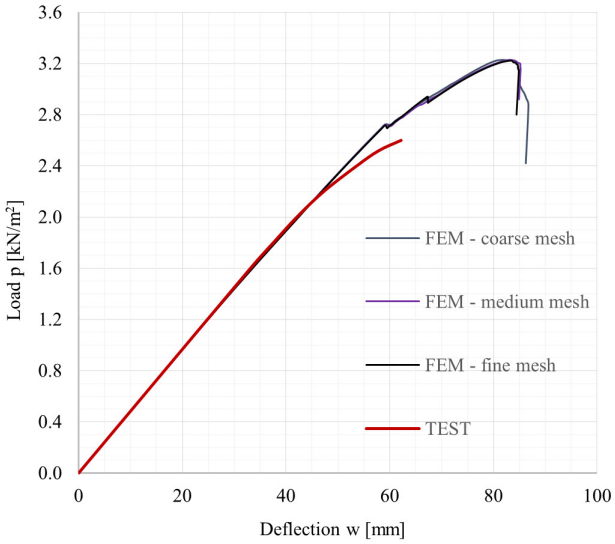

Fig. 12 Load-deflection dependence obtained by FEM and by test

point. The failure occurs as a consequence of the buckling of the top flange, whereby a concave dent is formed at the bend between the web and the top flange and a convex dent on the top flange. Such mode of failure corresponds with all the experimentally tested specimens.

These considerations led to the idea of introducing the effects of imperfections into the numerical model, the form of which would be analogous to deformations at failure.

3.4 Introduction of imperfection effects

Most researchers, when developing numerical models based on the nonlinear analysis, consider the influence of geometric imperfections (GI) based on the recommendations of the standard CEN EN 1993-1-5:2024 [36] According to it, the influence of GI can be numerically modeled based on the obtained critical buckling shapes using the linear buckling analysis. New European standard CEN EN 1993-1-14:2025 [25], recommends the use of equivalent geometric imperfections (EGI) when modeling plate and shell structures, unless more detailed GI testing and measurement is performed beforehand. In [22], the authors analyzed the specimen of the same type of HPS, where the initial imperfections were introduced via the 1st mode of buckling shape. Based on the analysis of the obtained results, and the results of the experimental analysis done within this research, it is concluded that the failure modes obtained in the research [22] do not fully correspond with the experimentally obtained failure modes. When defining the imperfection using the 1st mode of buckling shape in the paper [22], the imperfection was introduced only to the middle flange, which proved to be insufficiently accurate.

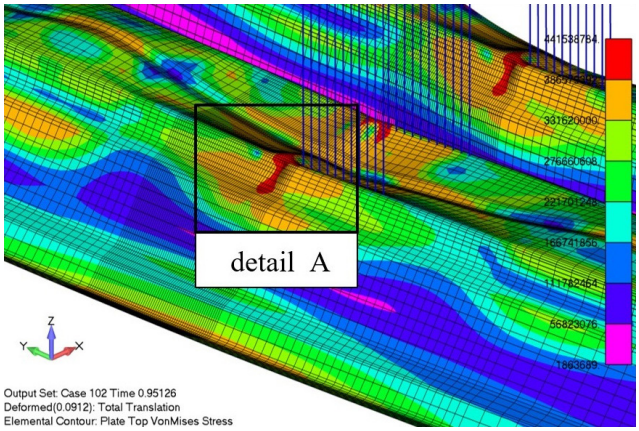

(a)

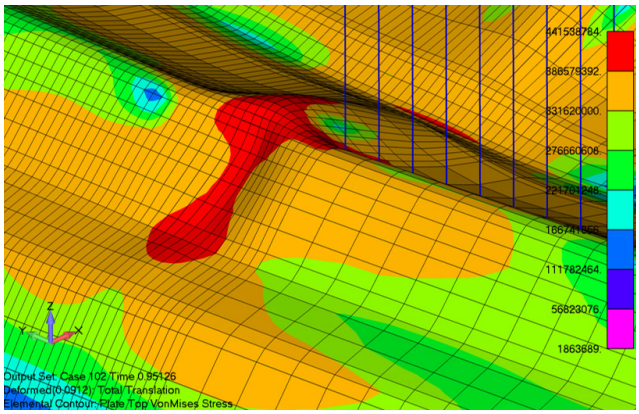

(b)

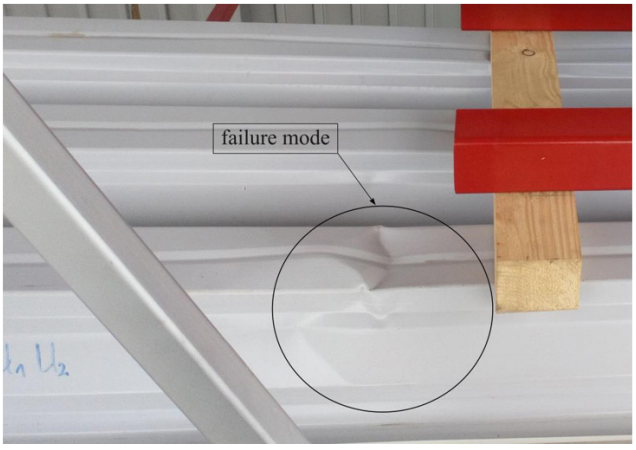

(c)

Fig. 13 Appearance and location of failure: (a) FEM analysis, (b) FEM analysis – detail A, (c) test

The standard CEN EN 1993-1-6:2025 [37] states that when analyzing shell structures using geometrically and materially nonlinear analysis with imperfections (GMNIA), EGI can also be introduced by forming local dimples. Within the conducted research, this method of introduction of imperfections is adopted in the paper. In this case the size of the local dimple showed according to be [37]:

$$\Delta w_{0,eq} > n_i \cdot t \cdot U_n;\ \Delta w_{0,eq} > 0.46 \text{ mm};\quad (1)$$

where:

- t is local shell thickness (t = 0.74 mm),
- n_i is a multiplier to achieve an appropriate tolerance level (recommended value of n_i is 25),
- U_n is dimple imperfection amplitude parameter for the relevant fabrication tolerance (recommended value of U_n for class C is 0.025).

The dimples are located in places where the denting at failure occurs, on the FE model without imperfections (B120 N4). In this model, it was determined that the failure occurs at the bending between the web and the top flange, at a distance of about 20 mm from the point of load application (Fig. 13 (a), (b)). The shapes of the introduced dimples correspond to the failure shape of the representative numerical model and the tested sample (B120 N4), which was used for further analysis. The dimples are introduced by displacing the nodes of the FE mesh so as to form a parabolic convex dent on the top flange and a parabolic concave dent on the web (Fig. 14). A total of 65 nodes were moved, and the values of node displacement for the unit value of imperfection (EGI = 1) are shown in Table 6.

As the initial assumed value of EGI, a higher value than that obtained by Eq. (1) was adopted, i.e., an EGI value of 0.5 mm was assumed. The EGI adopted in such manner was introduced at all transitions of the web into the top flange in the same cross-section.

Based on the obtained results for EGI = 0.5 mm (Fig. 15, curve: "FEM – EGI = 0.5 mm"), it is concluded that the imperfection obtained by the standard CEN EN 1993-1-6:2025 [37] is not satisfactory in terms of results accuracy. The load-bearing capacity obtained by FEM is 3.0 kN/m^2, and that obtained experimentally is 2.6 kN/m^2, which necessitates an increase of EGI. In order to find an appropriate imperfection size, numerical models with EGI = 1, 2, 3, 4 mm were analyzed.

By scaling the imperfection values given in Table 6, by values of EGI = 0, 0.5, 1, 2, 3 and 4 mm respectively, the corresponding node displacements were obtained. Thus, six numerical models were obtained, where EGI = 0 mm represents the initial model without imperfection.

The comparative results in the form of load-deflection (p-w) diagrams obtained by numerical and experimental analysis are shown in Fig. 15. The area between the experimental and the corresponding numerical diagrams was adopted as a parameter for determining the deviation of the numerical analysis results from the experimental analysis results. Based on the obtained areas, a diagram of the deviation of the FEM and experimental analysis results depending on the size of the imperfection was formed (Fig. 16). The minimum deviation

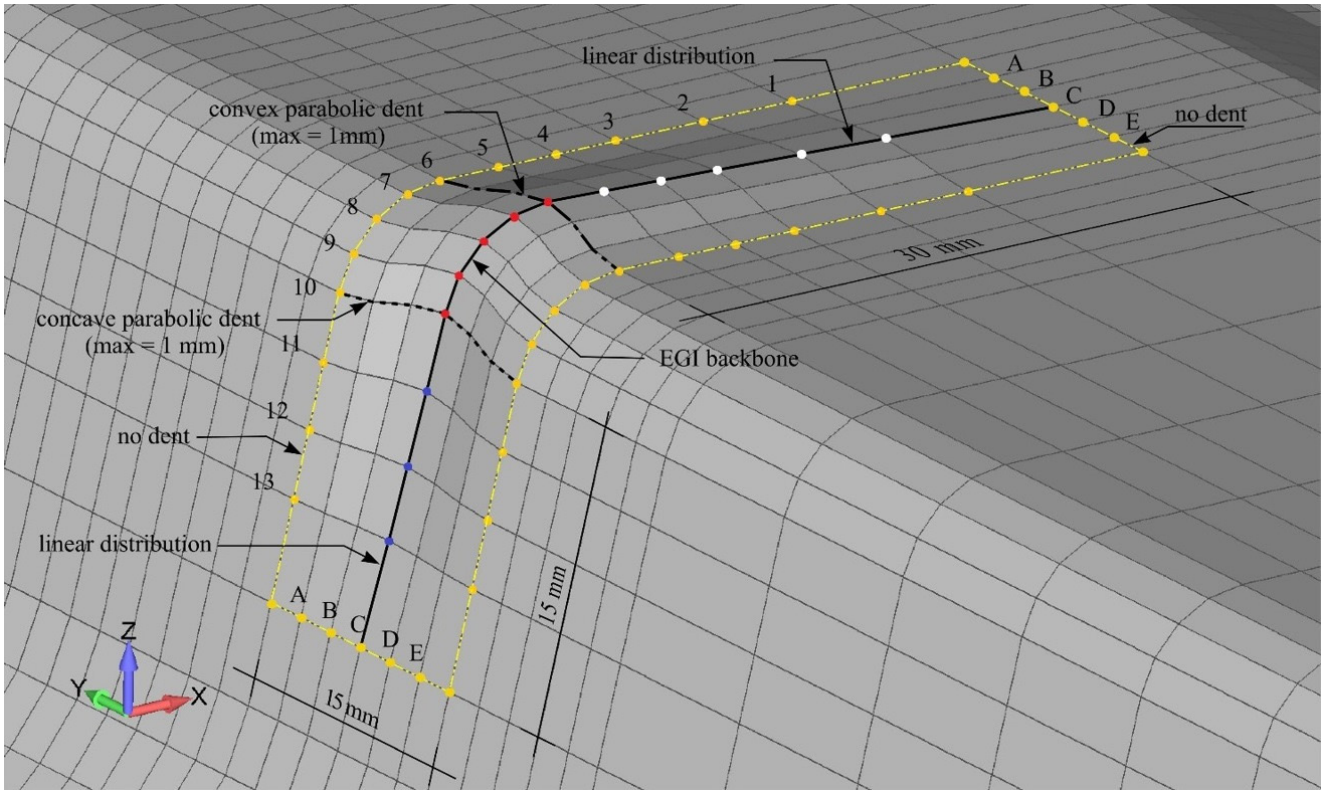

Fig. 14 Presentation of the performed imperfection on the model – EGI detail = 1.0 mm

Table 6 Values of node displacement when forming EGI on the model

Displacement direction (axis)	Designation of the node in FE mesh (Fig. 14) / Given displacement of the node, at EGI = 1.0				
	A1	B1	C1	D1	E1
X	0.083	0.250	0.333	0.250	0.083
	A2	B2	C2	D2	E2
X	0.125	0.375	0.500	0.375	0.125
	A3	B3	C3	D3	E3
X	0.167	0.500	0.667	0.500	0.167
	A4	B4	C4	D4	E4
X	0.194	0.582	0.777	0.582	0.194
	A5	B5	C5	D5	E5
X	0.222	0.667	0.889	0.667	0.222
	A6	B6	C6	D6	E6
X	0.25	0.75	1.0	0.75	0.25
	A7	B7	C7	D7	E7
X	0.25	0.75	1.0	0.75	0.25
	A8	B8	C8	D8	E8
X	0.25	0.75	1.0	0.75	0.25
Z	0.25	0.75	1.0	0.75	0.25
	A9	B9	C9	D9	E9
Z	0.25	0.75	1.0	0.75	0.25
	A10	B10	C10	D10	E10
Z	0.25	0.75	1.0	0.75	0.25
	A11	B11	C11	D11	E11
Z	0.194	0.583	0.777	0.583	0.194
	A12	B12	C12	D12	E12
Z	0.138	0.416	0.554	0.416	0.138
	A13	B13	C13	D13	E13
Z	0.083	0.248	0.331	0.248	0.083

of the numerical and experimental results is obtained for the EGI size of 3.02 mm. Based on this, the critical EGI size of 3.0 mm was adopted for further analysis.

4 Comparative analysis of FEM results (GMNIA) and the experimental test

The adopted form and critical size of the EGI were implemented in all models that were experimentally tested (Table 1) and the GMNIA analysis was performed. The comparative results of FEM and experimental results are shown in Table 7.

From the Table 7, it can be seen that the results obtained by the test and the FEM analysis are in very good agreement, both for the ultimate limit state (ULS) and the serviceability limit state (SLS), for the $L/200$ deflection. The obtained deviations of the results for the ULS case are up to 2.2%, and for the SLS case up to 3.8%.

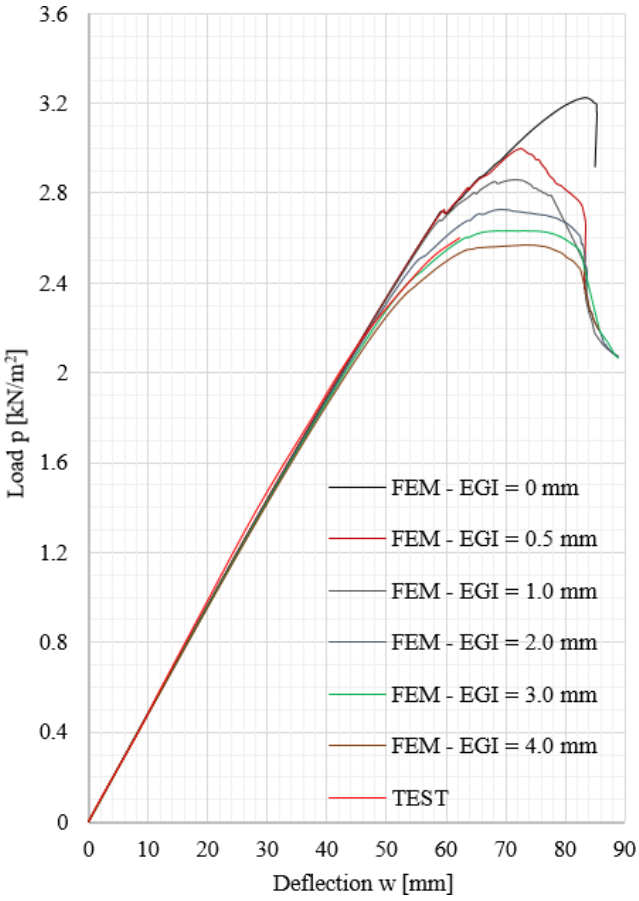

Fig. 15 The *p-w* diagram obtained by the test and by FEM with the varied size of EGI

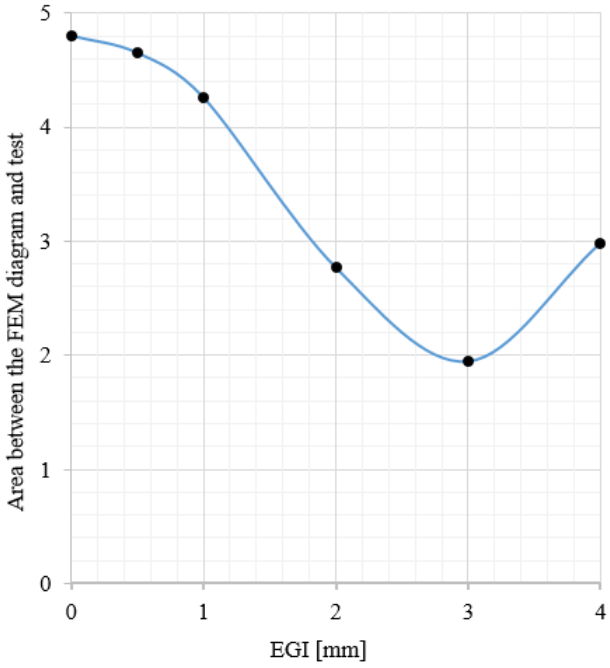

Fig. 16 Deviation of the results between the *p-w* curves obtained by FEM and test in the function of EGI size

Comparative load-deflection diagrams for the test and numerical results of the analyzed HPS with four fasteners

Table 7 Comparative results obtained by test and by FEM

	Specimen – model label						
	B40 N4	B80 N4	B120 N4	B160 N4	B200 N4	B160 N8	B200 N8
p_{ult} [kN/m^2] [TEST]	2.6	2.6	2.6	2.7	2.7	2.7	2.8
p_{ult} [kN/m^2] [FEM]	2.61	2.61	2.63	2.64	2.66	2.71	2.79
Δp_{ult} [%]	0.4	0.4	1.2	−2.2	−1.5	0.4	−0.4
w_{pult} [mm] TEST]	64.5	63.7	62.2	66.0	64.7	59.9	62.6
w_{pult} [mm] [FEM]	65.2	64.1	67.9	67.8	68.6	67.2	71.5
Δw_{pult} [%]	1.1	0.6	9.2	2.7	6	12.2	14.2
p_{200} [kN/m^2] [TEST]	1.42	1.45	1.45	1.47	1.48	1.52	1.58
p_{200} [kN/m^2] [FEM]	1.42	1.42	1.43	1.44	1.44	1.48	1.52
Δp_{200} [%]	0.0	−2.1	−1.4	−2.0	−2.7	−2.6	−3.8

Legend: p_{ult} – ultimate load; w_{pult} – corresponding deflection; p_{200} – max. load at $L/200$ deflection

in the connection and the contact length of 40, 80, 120, 160 and 200 mm are given in Fig. 17 (a), and for the specimens and models with eight fasteners in the connection and the contact length of 160 and 200 mm in Fig. 17 (b).

The presented diagrams show a complete agreement between the results of the test and FEM analysis. Nevertheless, this agreement should be taken with a certain reserve, because of the insufficiently researched experimental behavior of sheet metal after the ultimate load.

On the other hand, the conducted research provided an adequate (detailed) presentation of the local phenomena. The deformations at the location of failure and the support location are shown in Figs. 18 (a), (b) and 19 (a), (b). The Figs. 18 and 19 show a high similarity between the deformation shapes obtained by experimental testing and the application of FEM. A characteristic failure mode is shown, which is valid for all analyzed support conditions.

Based on the observations made, it can be considered that the proposed shape and size of the imperfections led to the successful validation of the developed FEM.

5 Conclusions

The paper presents the procedure for developing a numerical model for determining the strength of girders made of high-profiled sheets metal. As part of the model development, the procedure for modeling the HPS, supports, loads

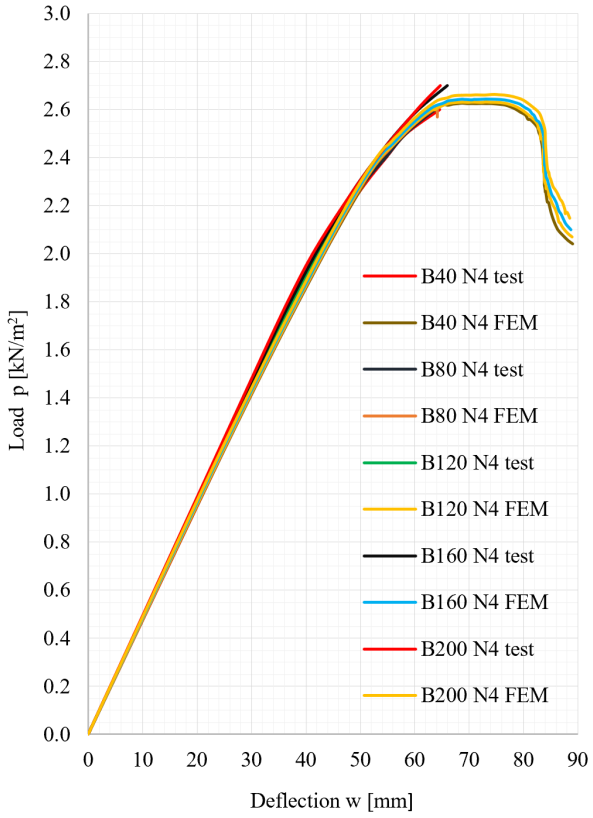

(a)

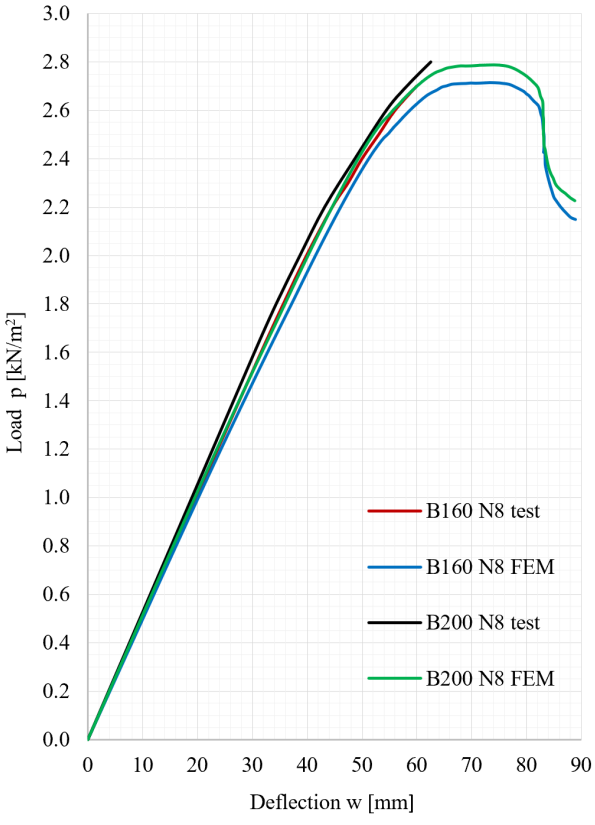

(b)

Fig. 17 Load-deflection diagrams obtained by test and FEM: (a) B40…120 N4; (b) B160…200 N8

(a)

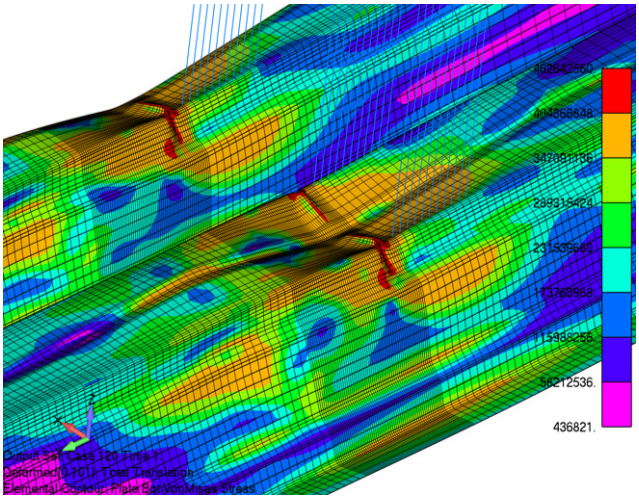

(b)

Fig. 18 Failure mode of the B200 N4 at limit load with zones of local buckling: (a) test specimen, (b) FE model

and boundary conditions, as well as material models, is presented. Based on the conducted model analyses with different FE mesh densities, the model was verified. After the verification, the results of FEM without imperfections and experimental analysis were compared. The comparison showed large deviations, which indicated that it was necessary to introduce sheet metal imperfections into the numerical model. Accordingly, the developed model included geometric and material nonlinear analysis with imperfections (GMNIA). Equivalent geometric imper-fections (EGI) were applied, in accordance with the recommendations of the standard CEN EN 1993-1-6:2025 [37]. As part of the research, it was proposed to introduce a new EGI shape, whose shape, position and size of which were determined based on the failure mode obtained by FEM and experimental analysis. After calibrating the size of the proposed EGI shape, it was shown that the required EGI size is far greater than the value proposed by the standard CEN EN 1993-1-6:2025 [37], which indicates the need to review the existing regulations.

(a)

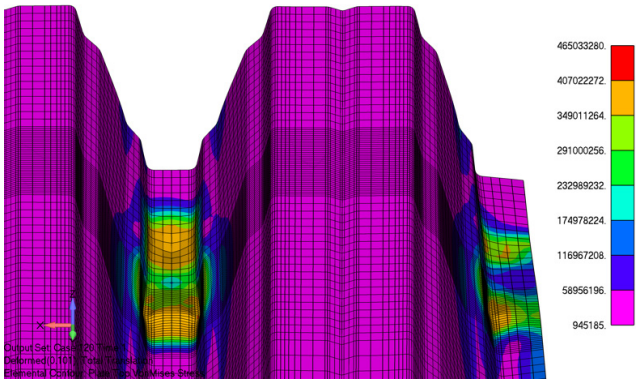

(b)

Fig. 19 Support deformation (B200 N4) at limit load, with local failure zones: (a) test specimen, (b) FE model

In order to reliably validate the proposed numerical model, parameters related to the support conditions of the HPS beam (sheet contact length, number and arrangement of fasteners) were also varied.

A comparative analysis of the obtained results of the experimental analysis and the FEM GMNIA analysis showed a very good agreement.

Also, the developed numerical model facilitated an adequate presentation and exact reproduction of local phenomena which are the result of buckling. It was determined that the failure of HPS girders occurs in all cases due to local buckling and wrinkling of the compressed flanges approximately at the midspan. This indicates that the loss of stability is the main cause of failure.

The presented numerical model provides far greater opportunities for analyzing the mechanical behavior of these and similar products compared to available analytical solutions, and at a much lower cost compared to experimental testing. Nevertheless, certain simplifications were introduced into the numerical model during modeling, which constitutes a partial lose of the model fidelity and accuracy of results, but also the compromise for the future users in engineering practice. The existence of horizontal forces in the connection, and

their potential impact on the magnitude of introduced imperfections should certainly be investigated in future research.

Future research also needs to be conducted on a larger number of models and experiments, which contain the results and post-failure behavior. This would facilitate a more complete presentation of the global behavior of HPS, thus contributing to potential optimization and a more accurate systematization of data regarding the HPS load-bearing capacity.

Acknowledgements

This research was supported by the Ministry of Science, Technological Development and Innovation of the Republic of Serbia, under the Agreement on Financing the Scientific Research Work of Teaching Staff at the Faculty of Civil Engineering and Architecture, University of Niš - Registration number: 451-03-34/2026-03/200095 dated 05/02/2026. The authors would also like to thank to the company: "Nešović produkt" in Međuhana, Serbia and "INM" in Arilje, Serbia.

The research is in line with the goals of sustainable development: 9 Industry, innovation and infrastructure, 11 Sustainable cities and communities.

References

[1] Hofmeyer, H., Geers, S. W. A., Snijder, H. H., Schafer, B. W. "The Direct Strength Method for first generation trapezoidal steel sheeting under Interior One Flange and Interior Two Flange web crippling", Thin-Walled Structures, 180, 109795, 2022. https://doi.org/10.1016/j.tws.2022.109795

[2] Vacev, T., Zorić, A., Ranković, S., Milić, M., Paunović, S., Nešović, I. "Analysis of Stressed Skin Behaviour of a Steel Façade Frame Under Varying Structural Conditions", International Journal of Steel Structures, 21, pp. 178–201, 2021. https://doi.org/10.1007/s13296-020-00425-2

[3] Vacev, T., Zorić, A., Milić, M., Paunović, S., Nešović, I. "Stressed Skin Design Versus Braced Frame Design Through Efficient Numerical Modelling", International Journal of Steel Structures, 20(4), pp. 1209–1229, 2020. https://doi.org/10.1007/s13296-020-00352-2

[4] American Iron and Steel Institute "AISI S100-16 North American specification for the design of cold-formed steel structural members", AISI, Washington, DC, USA, 2016.

[5] AS/NZS "AS/NZS 4600:2018 Cold-formed Steel Structures", Australian/New Zealand Standard, Sydney, Australia, Wellington, New Zealand, 2018.

[6] CEN "CEN EN 1993-1-3:2006 Eurocode 3 - Design of steel structures – Part 1–3: General rules – Supplementary rules for cold-formed members and sheeting", European Committee for Standardization, Brussels, Belgium, 2006.

[7] Aktepe, R., Erkal, B. G. "State-of-the-art review on measurement techniques and numerical modeling of geometric imperfections in cold-formed steel members", Journal of Constructional Steel Research, 207, 107942, 2023. https://doi.org/10.1016/j.jcsr.2023.107942

[8] Ahmed, H. S. S., Ghosh, S., Mangal, M. "Probabilistic estimation of the buckling strength of a CFS lipped-channel section with Type 1 imperfection", Thin-Walled Structures, 119, pp. 447–456, 2017. https://doi.org/10.1016/j.tws.2017.07.001

[9] Zeinoddini, V. M. Schafer, B. W. "Simulation of geometric imperfections in cold-formed steel members using spectral representation approach", Thin-Walled Structures, 60, pp. 105–117, 2012 https://doi.org/10.1016/j.tws.2012.07.001

[10] Koh, H., Blum, H. B. "A review of current practice for testing by analysis of cold-formed steel structures", Structures, 37, pp. 871–880, 2022. https://doi.org/10.1016/j.istruc.2022.01.017

[11] Radwan, M., Kövesdi, B. "Equivalent Geometric Imperfections for Local Buckling of Slender Box-section Columns", Periodica Polytechnica Civil Engineering, 65(4), pp. 1279–1287, 2021. https://doi.org/10.3311/PPci.18545

[12] Radwan, M., Kövesdi, B. "Monte Carlo Simulations for Global and Local Interaction Buckling of Welded Box-sections", Periodica Polytechnica Civil Engineering, 68(3), pp. 937–945, 2024. https://doi.org/10.3311/PPci.23475

[13] Schafer, B. W., Li, Z., Moen, C. D. "Computational modeling of cold-formed steel", Thin-Walled Structures, 48(10–11), pp. 752–762, 2010. https://doi.org/10.1016/j.tws.2010.04.008

[14] Schafer, B. W., Peköz, T. "Computational modeling of cold-formed steel: characterizing geometric imperfections and residual stresses", Journal of Constructional Steel Research, 47(3), pp. 193–210, 1998. https://doi.org/10.1016/S0143-974X(98)00007-8

[15] Šorf, M., Jandera, M. "Trapezoidal sheet hangers and concentrated or linear load distribution in profiled sheeting", ce/papers, 1(2–3), pp. 1563–1570, 2017. https://doi.org/10.1002/cepa.199

[16] Raebel, C. H., Gwodzdz, D. "Comparison of Experimental and Numerical Results for Flexural Capacity of Light-Gage Steel Roof Deck", In: 24th International Specialty Conference on Cold-Formed Steel Structures, St. Louis, MO, USA, 2018, pp. 55–67. [online] Available at: https://scholarsmine.mst.edu/isccss/24iccfss/session1/4 [Accessed: 24 March 2025]

[17] Casafont, M., Marimon, F., Bové, O., Ferrer, M., Centelles, X. "Local buckling of cold-formed steel trapezoidal sheets: Data for finite element model validation", Data in Brief, 53, 110075, 2024. https://doi.org/10.1016/j.dib.2024.110075

[18] Haidarali, M. R., Nethercot, D. A. "Finite element modelling of cold-formed steel beams under local buckling or combined local/distortional buckling", Thin-Walled Structures, 49(12), pp. 1554–1562, 2011. https://doi.org/10.1016/j.tws.2011.08.003

[19] Degtyarev, V. V. "A Finite Element Study of Corrugated Steel Deck Subjected to Concentrated Loads", In: 24th International Specialty Conference on Cold-Formed Steel Structures, St. Louis, MO, USA, 2018, pp. 729–743.

[20] Degtyarev, V. V. "Concentrated load distribution in corrugated steel decks: A parametric finite element study", Engineering Structures, 206, 110158, 2020. https://doi.org/10.1016/j.engstruct.2019.110158

[21] Degtyarev, V. V. "Finite element modeling of cold-formed steel deck in bending", Magazine of Civil Engineering, 94(2), pp. 129–144, 2020. https://doi.org/10.18720/MCE.94.11

[22] Vacev, T., Nešović, I., Milić, M., Zorić, A., Paunović, S. "Influence of Support Conditions on Single-Span Profiled Sheet Metal Strength Through Nonlinear FEM Analysis", International Journal of Steel Structures, 20, pp. 1302–1318, 2020. https://doi.org/10.1007/s13296-020-00361-1

[23] Rzeszut, K., Szumigała, T. "Optimal design methods of trapezoidal steel sheets", In: AIP Conference Proceedings, 2060(1), 020011, 2019. https://doi.org/10.1063/1.5086142

[24] Jurdová, K. "Limit State of Trapezoidal Metal Sheets Exposed to Concentrated Load", International Journal of Civil and Environmental Engineering, 7(10), pp. 724–728, 2013.

[25] CEN "CEN EN 1993-1-14:2025 Eurocode 3- Design of steel structures – Part 1-14: Design assisted by finite element analysis", European Committee for Standardization, Brussels, Belgium, 2025.

[26] Szumigała, T. "Experimental tests of second generation trapezoidal sheets", In: Modern Trends in Research on Steel, Aluminium and Composite Structures, pp. 192–198, Routledge, 2021. ISBN 978-0-367-67637-7 https://doi.org/10.1201/9781003132134-22

[27] Zakhimi, H. H., Hofmeyer, H., Snijder, H. H. B., Mahendran, M. M. "Explicit and interaction direct strength methods for combined web crippling and bending moment failure of first-generation trapezoidal steel sheeting", Thin-Walled Structures, 157, 106927, 2020. https://doi.org/10.1016/j.tws.2020.106927

[28] Willems, D. W. C., Hofmeyer, H., Snijder, H. H., Schafer, B. W. "The direct strength method for combined bending and web crippling of second-generation trapezoidal steel sheeting", Thin-Walled Structures, 167, 108149, 2021. https://doi.org/10.1016/j.tws.2021.108149

[29] Dogar, A. U. R. "Post Elastic Behaviour and Moment Redistribution in a Double Span LTP200 Steel Trapezoidal Sheet", MSc Thesis, Luleå University of Technology, 2018. [online] Available at: https://urn.kb.se/resolve?urn=urn%3Anbn%3Ase%3Altu%3Adiva-68306 [Accessed: 26 March 2025]

[30] Weckman Steel Oy "Weckman Catalogue", Vierumäki, Finland, 2020.

[31] Weckman "Weckman Optimi, (Optimi 4.4v2)", [computer program] Available at: https://www.weckmansteel.fi/en/download-optimi/ [Accessed: 20 March 2025]

[32] Siemens "Femap with NX Nastran, (v11.0.1 64-bit)", [computer program] Available at: https://community.sw.siemens.com/s/products [Accessed: 10 Jun 2024]

[33] Siddh, S. P., Patil, Y. D., Patil, H. S. "Experimental studies on behaviour of composite slab with profiled steel sheeting", Materials Today: Proceedings, 4(9), pp. 9792–9796, 2017. https://doi.org/10.1016/j.matpr.2017.06.268

[34] Casariego, P., Casafont, M., Ferrer, M., Marimon, F. "Analytical study of flat and curved trapezoidal cold formed steel sheets by means of the yield line theory. Part 1: Flat sheets without transverse corrugations", Thin-Walled Structures, 141, pp. 675–692, 2019. https://doi.org/10.1016/j.tws.2018.12.017

[35] Dogar, A. U. R., Rehman, H. M. U. U., Tafsirojjaman, T., Iqbal, N. "Experimental investigations on inelastic behaviour and modified Gerber joint for double-span steel trapezoidal sheeting", Structures, 24, pp. 514–525, 2020. https://doi.org/10.1016/j.istruc.2020.01.042

[36] CEN "CEN EN 1993-1-5:2024 Eurocode 3- Design of steel structures – Part 1–5: Plated structural elements", European Committee for Standardization, Brussels, Belgium, 2024.

[37] CEN "CEN EN 1993-1-6:2025 Eurocode 3- Design of steel structures – Part 1–6: Strength and stability of shell structures", European Committee for Standardization, Brussels, Belgium 2025.